

Nonequilibrium entanglement between levitated masses under optimal control

Alexander N. Poddubny,^{1,*} Klemens Winkler,² Benjamin A. Stickler,³
Uroš Delić,⁴ Markus Aspelmeyer,^{4,5} and Anton V. Zasedatelev^{4,†}

¹*Department of Physics of Complex Systems, Weizmann Institute of Science, Rehovot 7610001, Israel*

²*Vienna Center for Quantum Science and Technology (VCQ),*

Faculty of Physics & Vienna Doctoral School in Physics, University of Vienna, A-1090 Vienna, Austria

³*Institute for Complex Quantum Systems, Ulm University,
Albert-Einstein-Allee 11, D-89069 Ulm, Germany*

⁴*Vienna Center for Quantum Science and Technology (VCQ), Faculty of Physics,
University of Vienna, Boltzmannngasse 5, A-1090 Vienna, Austria*

⁵*Institute for Quantum Optics and Quantum Information (IQOQI) Vienna,
Austrian Academy of Sciences, Boltzmannngasse 3, 1090 Vienna, Austria*

(Dated: August 13, 2024)

We present a protocol that maximizes unconditional entanglement generation between two masses interacting directly through $1/r^n$ potential. The protocol combines optimal quantum control of continuously measured masses with their non-equilibrium dynamics, driven by a time-dependent interaction strength. Applied to a pair of optically trapped sub-micron particles coupled via electrostatic interaction, our protocol enables unconditional entanglement generation at the fundamental limit of the conditional state and with an order of magnitude smaller interaction between the masses compared to the existing steady-state approaches.

The progress in optomechanics [1–3] enables quantum state preparation of individual large-mass systems [4–8] and long-range cavity-mediated entanglement generation [9, 10]. In addition to offering a valuable resource in quantum sensing and metrology [2, 11], entanglement between macroscopic systems holds conceptual significance for fundamental research. Being mediated via direct physical interaction through Coulomb, Casimir or the Newtonian force, it will facilitate the search for dark matter [12–14], the exploration of physics beyond the standard model [15], and might eventually provide insights into the question of whether the gravitational interaction is fundamentally quantum or not [16, 17].

However, the cavity-free entanglement generation between two masses poses significant experimental challenges [18, 19] and has yet to be achieved. Interactions with the environment rapidly destroy quantum correlations as the size and complexity of systems grows [11], posing the necessity for practical methods to enhance quantum correlations against large decoherence rates. Strategies such as reservoir engineering which involves coupling a macroscopic systems to nonequilibrium baths [20, 21] have been proposed to facilitate entanglement generation. Additionally, parametrically-driven interactions offer an innovative approach to achieve entanglement at higher temperatures, surpassing the need for deep cooling toward the ground state [22–24]. By driving systems out of their thermal equilibrium, e.g. through a modulated interaction between subsystems, one can break the thermodynamic limit of the entanglement $k_B T \ll \hbar\omega$ (with $\hbar\omega$ being the typical energy of the system) [22, 25]. While this methodology has primarily been developed for cavity optomechanical systems, recent theoretical work explores entanglement generation

in free space through weak forces, suggesting protocols based on squeezing the motion of large masses [19, 26].

In this work, we combine methods of nonequilibrium entanglement generation with the time-continuous quantum control [27] of two harmonically trapped masses interacting in free space. We leverage continuous measurement and feedback with a periodic modulation of the interaction to drive the system into a non-equilibrium state that exhibits strong unconditional entanglement. We show how an optimal quantum measurement can be performed to generate entanglement in the conditional state [28]. Following this strategy, we connect the observable entanglement to the properties of the measurement apparatus [27]. Then we use feedback control to stabilize the effective temperature of the motion, thus optimizing entanglement likelihood through a specifically chosen cost function. Ultimately, our protocol achieves unconditional (*out-of-loop*) entanglement between the motion of directly interacting masses at the fundamental limit of their joint conditional state.

We consider two identical particles with mass m , each confined in one spatial dimension by a harmonic potential with eigenfrequency Ω_0 as in Ref. [28]. The particles are modeled to interact via a central potential of the form k/r^n , e.g. via gravitation, electrostatic or Casimir interaction, where we introduce $r = \sqrt{x_{\text{zpf}}^2 (X_1 - X_2)^2 + R^2}$ with particle positions X_k . Here, R denotes the interparticle distance along a spatial direction orthogonal to the motion $X_{1,2}$ with $x_{\text{zpf}} = \sqrt{\hbar/m\Omega_0}$. In the limit of small displacements and considering terms up to quadratic order in position yields the interaction Hamiltonian $H_{\text{int}} = \hbar g (X_1 - X_2)^2$ with a coupling rate $g = k/(2nR^{2+n}m\Omega_0)$. For the following discussion, we assume that the coupling rate can be temporally modu-

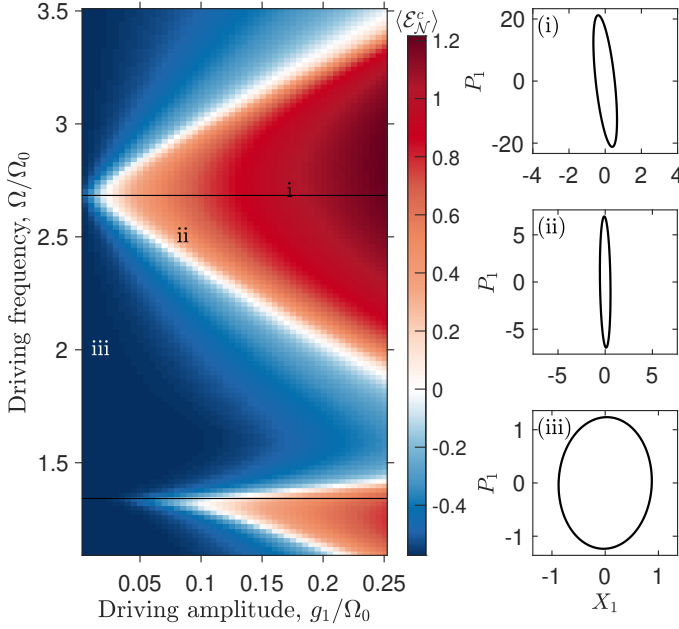


FIG. 1. Conditional period-averaged logarithmic negativity as the function of driving amplitude g_1 and modulation frequency Ω . Panels on the right illustrate the standard deviation of the bivariate Wigner distribution, given by the conditional covariance matrix Σ^c , depending on X_1 and P_1 for three characteristic values of $\{g_1/\Omega_0, \Omega/\Omega_0\} = \{0.17, 2.7\}, \{0.08, 2.5\}, \{0.01, 2.0\}$, labeled (i–iii) on the color plot. Here we use the following parameters of the system: $g_0/\Omega_0 = 0.2$, $\Gamma_{\text{ba}}/\Omega_0 = 5\%$, $\Gamma_{\text{th}}/\Gamma_{\text{ba}} = 5\%$ and $q = 0.1/\Omega_0$, fully consistent with the parameters in Ref. [28].

lated with the frequency Ω e.g. by varying the distance R , such that $g(t) = g_0 + 2g_1 \cos \Omega t$. Additionally, the particles are controlled individually by a feedback force u_k . The total Hamiltonian is then given by

$$H = \sum_{k=1,2} \frac{\hbar\Omega_0}{2} (X_k^2 + P_k^2) - \sum_{k=1,2} \hbar X_k u_k(t) + \hbar g(t) (X_1 - X_2)^2. \quad (1)$$

In the rotating reference frame, the parametric modulation of the coupling $g(t)$ leads to the term $\propto (a_1^\dagger a_2^\dagger - a_1 a_2)$ [29, 30], where $a_{1,2}$ are the annihilation operators for the oscillator motion. This term describes two-mode squeezing and entanglement generation.

Relevant decoherence channels include thermal decoherence from residual gas and photon recoil with rates Γ_{th} and Γ_{ba} respectively. These settings are typical for various continuously measured interferometric arrangements, such as optical trapping of sub-micron particles in ultra-high vacuum, which offers extreme isolation, scalability, and potential for landscape engineering [3].

Continuous position measurement of each particle, e.g. via homodyne detection, conditions the system on the measured photocurrents, leading to the conditional state represented by the density matrix ρ_c . With Gaussian ini-

tial states and the linear dynamics following from Eq. 1, the conditional state remains Gaussian, fully described by its first and second moments.

Using $X_{1,2}$ and dimensionless momenta $P_{1,2}$ we define $\mathbf{X} = (X_1, P_1, X_2, P_2)^T$, the conditional mean values $\mathbf{X}_c := \text{Tr}[\mathbf{X}\rho_c] = \langle \mathbf{X} \rangle_c$ and the covariance matrix $\Sigma_{kl}^c = \langle X_k X_l \rangle_c - \langle X_k \rangle_c \langle X_l \rangle_c$.

Following the notations from [28], with the time-modulated drift matrix $\mathbf{A}(t)$

$$\mathbf{A}(t) = \begin{pmatrix} 0 & \Omega_0 & 0 & 0 \\ -\Omega_0 - 2g(t) & -\gamma & 2g(t) & 0 \\ 0 & 0 & 0 & \Omega_0 \\ 2g(t) & 0 & -\Omega_0 - 2g(t) & -\gamma \end{pmatrix}. \quad (2)$$

the evolution of the systems conditional mean values and covariance matrix is described by

$$d\mathbf{X}_c(t) = \mathbf{A}(t)\mathbf{X}_c(t)dt + \mathbf{B}\mathbf{u}(t)dt + \Sigma^c(t)\mathbf{C}^T\mathbf{W}^{-1}d\mathbf{w}(t) \quad (3a)$$

$$d\Sigma^c = \mathbf{A}(t)\Sigma^c(t)dt + \Sigma^c(t)\mathbf{A}(t)^T dt + \mathbf{V}dt - \Sigma^c(t)\mathbf{C}^T\mathbf{W}^{-1}\mathbf{C}\Sigma^c(t)dt \quad (3b)$$

with control matrix \mathbf{B} , input force vector $\mathbf{u} = (u_1, u_2)^T$, measurement matrix \mathbf{C} , system and measurement noise correlation matrices \mathbf{V} and \mathbf{W} and stochastic vector $d\mathbf{w}(t) = (dW_1(t), dW_2(t))^T$.

Making the strong interferometric measurement of the position quadrature unavoidably perturbs the system, causing it to explore a larger phase space. Subject to excess noise, the averaged conditional state turns into the unconditional state of the system $\rho = \mathbb{E}[\rho_c]$ [27]. The covariance matrix of the unconditional state is given by the sum of the conditional state and the excess noise $\Sigma^u = \Sigma^c + \Xi^{\text{ex}}$.

To minimize excess noise, we apply the theoretical framework of classical control theory with the Kalman-Bucy filter as optimal observer together with a linear quadratic regulator (LQR) as optimal controller for minimizing the cost function $\mathcal{J} = \int \mathbb{E}[\mathbf{X}_c^T \mathbf{P} \mathbf{X}_c + \mathbf{u}^T q \mathbf{u}] dt$, with the cost matrix \mathbf{P} and the control effort q [31, 32]. From now on, we will use the Einstein-Podolsky-Rosen (EPR) cost function, which minimizes EPR-type variances in the joint phase space of the two particles, as detailed in Ref. [28].

The optimal feedback $\mathbf{u}(t) = -\mathbf{K}(t)\mathbf{X}_c(t)$ is determined by the feedback gain $\mathbf{K}(t) = \mathbf{B}^T \Omega(t)/q$, solving the backwards Riccati equation

$$d\Omega(t) = -\mathbf{A}^T(t)\Omega(t) - \Omega(t)\mathbf{A}(t)dt - \mathbf{P}dt + \Omega(t)\frac{\mathbf{B}\mathbf{B}^T}{q}\Omega(t)dt. \quad (4)$$

The excess noise matrix Ξ^{ex} depends on both, the measurement setup and the feedback from the controller, it's time evolution is governed by [27]

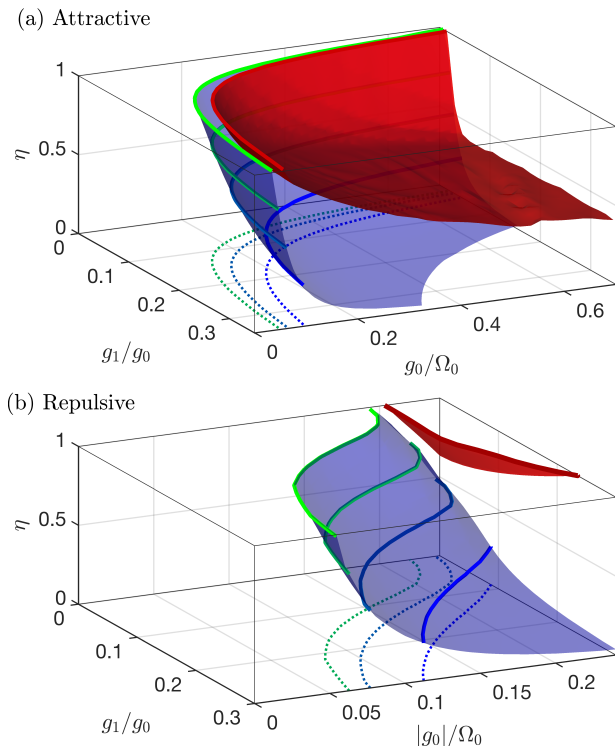


FIG. 2. The boundary for the conditional and unconditional time-averaged entanglement is shown by the blue and dark red surfaces, respectively. The case of attractive interaction $g_0 > 0$ (a) and repulsive interaction $g_0 < 0$ (b). All calculations are done for the EPR phase $\varphi = \pi$. The contour curves (solid) show the boundaries for unconditional entanglement calculated at $\eta = 0.25, 0.5, 0.75$ and 1 , with their projections illustrated by the dotted curves.

$$\begin{aligned}
 d\Xi^{ex}(t) &= (\mathbf{A} - \mathbf{BK}(t))\Xi^{ex}(t)dt \\
 &+ \Xi^{ex}(t)(\mathbf{A} - \mathbf{BK}(t))^T dt \\
 &+ (\Sigma^c(t)\mathbf{C}^T + \mathbf{M})\mathbf{W}^{-1}(\Sigma^c(t)\mathbf{C}^T + \mathbf{M})^T dt.
 \end{aligned} \quad (5)$$

Defining $\tilde{\nu}$ as the minimal symplectic eigenvalue of the either the matrix Σ^c or Σ^u , we employ the function $\mathcal{E}_{\mathcal{N}} = -\ln(2\tilde{\nu})$ to quantify the conditional and unconditional entanglement of the state respectively. States are detected as entangled if $\mathcal{E}_{\mathcal{N}} > 0$, connecting to the logarithmic negativity, a measure for entanglement, via $\max(0, \mathcal{E}_{\mathcal{N}})$ [33, 34].

We solve the periodic time-dependent Riccati equations using the Schur decomposition method [35]. In this approach, Eq. (3b) is described by the Hamiltonian matrix $\mathbb{H} = \begin{pmatrix} \mathbf{A}^T & -\mathbf{C}\mathbf{W}^{-1}\mathbf{C} \\ -\mathbf{V} & -\mathbf{A} \end{pmatrix}$. Next, we evaluate the Schur decomposition of the evolution operator over the modulation period $\mathbb{S} = \exp(\int_0^{2\pi/\Omega} \mathbb{H}(t)dt)$, $\mathbb{S} = \mathbf{U}\mathbf{\Lambda}\mathbf{U}^T$, where $\mathbf{\Lambda}$ is an upper-diagonal matrix and $\mathbf{U} = \begin{pmatrix} \mathbf{U}_{11} & \mathbf{U}_{12} \\ \mathbf{U}_{21} & \mathbf{U}_{22} \end{pmatrix}$ is the unitary one. The covariance matrix is then given by $\hat{\Sigma}^c(t) = \mathbf{U}_{12}(t)[\mathbf{U}_{11}(t)]^{-1}$. The brute-force evaluation

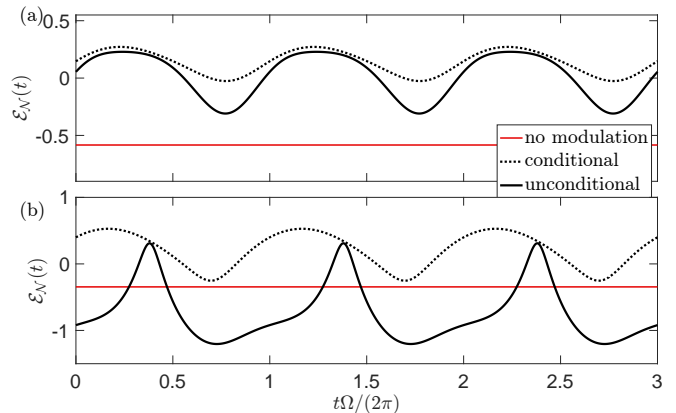


FIG. 3. Time-dependent logarithmic negativity $\mathcal{E}_{\mathcal{N}}(t)$ for (a) attractive case with $g_0/\Omega_0 = 0.2$ and (b) repulsive case with $g_0/\Omega_0 = -0.2$. Dotted black curves correspond to the conditional negativity, solid black curves correspond to the unconditional one. Horizontal solid lines show the values of $\mathcal{E}_{\mathcal{N}}(t)$ without the modulation, $g_1 = 0$. Calculated for $\Omega/\Omega_0 = 2.74$ (a) and $\Omega/\Omega_0 = 0.7$ (b).

of the S matrix leads to severe numerical errors for low values of control effort q and low modulation frequencies, since $\mathbb{H}(t)$ has eigenvalues with positive real part. This is in contrast to the Floquet engineering of closed quantum systems [36–39]. Although similar in form to S, Floquet Hamiltonians predominantly govern the unitary evolution of a wavefunction, thereby avoiding such issues. One workaround is provided by the so-called periodic QR decomposition [40–42]. In our experience, however, evaluating the $\mathbf{U}(t)$ dependence iteratively proved to be more numerically efficient [43].

According to the stationary theory under the attractive interaction $g_0 > 0$ [18], the motion of particles remains separable unless the interaction strength exceeds the mechanical frequency $g_0 \gtrsim \Omega_0$. Tailoring feedback control to maximize entanglement generation can help to lower the separability threshold. However, this approach still necessitates $g_0 \sim \Omega_0$ [28], which unfortunately stretches far beyond current experimental reach [44]. Therefore, realistic protocols should demonstrate a separability threshold at much lower interactions. We examine our protocol setting $g_0 = 0.2\Omega_0$, with the other parameters being the same as those considered in the stationary theory [28].

Figure 1 shows the conditional entanglement measure, logarithmic negativity $\langle \mathcal{E}_{\mathcal{N}}^c \rangle$, calculated as a function of the amplitude g_1 and frequency Ω of the modulation. Red color regions correspond to the entangled conditional state, where $\langle \mathcal{E}_{\mathcal{N}}^c \rangle > 0$. This happens at the parametric resonances, with the main resonant frequency being $\Omega = 2\Omega^*$, $2\Omega^* = 2\sqrt{\Omega_0^2 + 4\Omega_0 g_0} \approx 2.74\Omega_0$ for the chosen parameters. When the squeezing in the joint phase space is strong enough quantum correlations survive thermal fluctuations destroying it otherwise. Increasing the

modulation depth g_1 expands the entangled region. Furthermore, for sufficiently large g_1 , an additional parametric resonance emerges at the half of the drive frequency $\Omega = \Omega^*$. This result is well-known from the stability analysis of quantum systems under parametric drives [45]. The two-mode squeezing can also be achieved through parametric driving of the particle frequencies using the correct phase relation φ between the frequency drives $\Omega_m(t) = \Omega_0 + \Omega_1 \cos(\Omega_p t + \varphi)$. Here, a modulation of the interaction strength naturally ensures the perfect phases for optimal squeezing, which is evidenced in Fig. 1(i-iii). The panels (i-iii) illustrate the standard deviation of the corresponding Wigner function, characterized by the covariance matrix Σ^c of the conditional state, calculated for several characteristic values of $\{g_1, \Omega_1\}$.

Having established conditional entanglement generation via parametric modulation, we now explore a broader parameter space. The key parameters are the stationary interaction strength g_0/Ω_0 , the amplitude g_1/g_0 and frequency Ω/Ω_0 of the time-dependent interaction, and the detection efficiency η of the time-continuous position measurement. To present the calculated $\langle \mathcal{E}_N(g_0, g_1, \eta, \Omega) \rangle$ within a single plot, for every combination of $\{g_0, g_1, \eta\}$, we select the maximum logarithmic negativity at the frequency Ω , corresponding to the strongest parametric resonance in the system. Figure 2 shows the separability boundaries $\langle \mathcal{E}_N^u \rangle = 0$ obtained in the case of attractive (a) and repulsive (b) interaction. Here, we represent the performance of both conditional (blue surface) and unconditional states (red surface). We also plot contours on the surface of the conditional state for η equal to 0.25, 0.5, 0.75, and 1, along with projections on the (g_0, g_1) plane. In the attractive regime with relatively low modulation depth $g_1 = 0.2g_0$ and realistic detection efficiency of $\eta = 0.5$, our approach predicts entanglement generation at $g_0 = 0.1\Omega_0$. This is more than an order of magnitude lower in comparison to existing stationary protocols [18, 28]. Stationary entanglement in the repulsive case requires $|g_0| > 0.2\Omega_0$ [28], but the system turns unstable when $|g_0| \geq 0.25\Omega_0$, which makes it extremely hard to implement. The parametric drive of the interaction modifies fundamental limits of entanglement generation, making it possible under more relaxed experimental conditions, Fig. 2b.

The generation of time-averaged unconditional (*out-of-loop*) entanglement demands much higher detection efficiency with the given parameters and is likely to remain unattainable in the experiments. Nonetheless, optimal quantum control that minimizes the EPR cost function enables robust generation of unconditional entanglement in the stroboscopic regime, establishing quantum correlations beyond the separability criteria at a specific time. This protocol relies on the continuous time-resolved phase space tomography, fully consistent with the introduced measurement-based feedback control.

Figure 3 demonstrates the time dependence of the log-

arithmic negativity of unconditional states (black solid curves) for the attractive (a) and repulsive (b) regimes. For comparison, we also include the results without the modulation (red dotted lines) and the negativity of conditional states with modulation (black dotted curves). We observe a significant increase in the logarithmic negativity of the unconditional state, surpassing the separability boundary $\mathcal{E}_N^u = 0$, and approaching the fundamental limit of nonequilibrium entanglement. This is a remarkable result that allows for *out-of-loop* entanglement generation between large masses under realistic experimental conditions. Importantly, the peaking period of the unconditional entanglement is persistent with the period of parametric resonance $1/\Omega$. Similar phenomena have been observed in amplitude-modulated optomechanical systems, where the entanglement between the mirror motion and the cavity field oscillates with the period of the parametric drive [25].

Summary and outlook — We have developed a protocol for unconditional entanglement generation between two masses in free space interacting via $1/r^n$ potential. The protocol involves continuous monitoring and optimal state estimation via Kalman filtering as well as LQR feedback to enhance the entanglement between two oscillators under parametrically driven interaction. We developed feedback control strategy specifically tailored to maximize entanglement generation. It is achieved by the cost function of the linear quadratic regulator which minimizes EPR-variances of the particles' motion, as detailed in Ref.[28]. The feedback loop generates a non-equilibrium unconditional entanglement, significantly reducing the complexity for future experiments.

Our protocol achieves unconditional entanglement generation at the fundamental limit of the conditional state, ultimately making experimental implementation of the *out-of-loop* entanglement fairly accessible in laboratories. In particular, operating in an attractive regime with a gentle modulation depth of 20% and a realistic detection efficiency of 50%, we achieve entanglement at the interaction strength $g_0 = 0.1\Omega_0$ – more than an order of magnitude improvement over existing stationary protocols [18, 28]. These findings emphasize the potential of combining non-equilibrium dynamics with quantum control techniques to advance entanglement generation between macroscopic systems and setting the stage for future research with gravitational or Casimir interactions.

The authors thank Andreas Deutschmann-Olek, Henning Rudolph, Ayub Khodaei, Nancy Gupta, Nikolai Kiesel, Gerard Higgins and Corentin Gut for insightful discussions. K.W. and M.A. received funding from the European Research Council (ERC) under the European Union's Horizon 2020 research and innovation program (grant agreement No 951234), and from the Research Network Quantum Aspects of Spacetime (TURIS). BAS acknowledges funding by the DFG-510794108 as well as by the Carl-Zeiss-Foundation through the project QPho-

ton. U.D. acknowledges funding from the Austrian Science Fund (FWF, Project DOI 10.55776/I5111). A.V.Z. acknowledges support from the European Union's Horizon 2020 research and innovation programme under the Marie Skłodowska-Curie grant LOREN (grant agreement ID: 101030987).

* poddubny@weizmann.ac.il

† anton.zasedatelev@univie.ac.at

- [1] M. Aspelmeyer, T. J. Kippenberg, and F. Marquardt, Cavity optomechanics, *Reviews of Modern Physics* **86**, 1391 (2014).
- [2] S. Barzanjeh, A. Xuereb, S. Gröblacher, M. Paternostro, C. A. Regal, and E. M. Weig, Optomechanics for quantum technologies, *Nature Physics* **18**, 15 (2022).
- [3] C. Gonzalez-Ballester *et al.*, Levitodynamics: Levitation and control of microscopic objects in vacuum, *Science* **374**, eabg3027 (2021).
- [4] J. D. Teufel, T. Donner, D. Li, J. W. Harlow, M. Allman, K. Cicak, A. J. Sirois, J. D. Whittaker, K. W. Lehnert, and R. W. Simmonds, Sideband cooling of micromechanical motion to the quantum ground state, *Nature* **475**, 359 (2011).
- [5] J. Chan, T. M. Alegre, A. H. Safavi-Naeini, J. T. Hill, A. Krause, S. Gröblacher, M. Aspelmeyer, and O. Painter, Laser cooling of a nanomechanical oscillator into its quantum ground state, *Nature* **478**, 89 (2011).
- [6] U. Delic *et al.*, Cooling of a levitated nanoparticle to the motional quantum ground state, *Science* **367**, 892 (2020).
- [7] L. Magrini *et al.*, Real-time optimal quantum control of mechanical motion at room temperature, *Nature* **595**, 373–377 (2021).
- [8] F. Tebbenjohanns *et al.*, Quantum control of a nanoparticle optically levitated in cryogenic free space, *Nature* **595**, 378–382 (2021).
- [9] C. Ockeloen-Korppi *et al.*, Stabilized entanglement of massive mechanical oscillators, *Nature* **556**, 478–482 (2018).
- [10] R. Riedinger *et al.*, Remote quantum entanglement between two micromechanical oscillators, *Nature* **556**, 473–477 (2018).
- [11] F. Fröwis, P. Sekatski, W. Dür, N. Gisin, and N. Sangouard, Macroscopic quantum states: Measures, fragility, and implementations, *Rev. Mod. Phys.* **90**, 025004 (2018).
- [12] F. Monteiro, G. Afek, D. Carney, G. Krnjaic, J. Wang, and D. C. Moore, Search for composite dark matter with optically levitated sensors, *Phys. Rev. Lett.* **125**, 181102 (2020).
- [13] E. Kilian, M. Rademacher, J. M. H. Gosling, J. H. Iacoponi, F. Alder, M. Toroš, A. Pontin, C. Ghag, S. Bose, T. S. Monteiro, and P. F. Barker, Dark matter searches with levitated sensors (2024), arXiv:2401.17990 [quant-ph].
- [14] D. C. Moore and A. A. Geraci, Searching for new physics using optically levitated sensors, *Quantum Science and Technology* **6**, 014008 (2021).
- [15] A. Bassi, K. Lochan, S. Satin, T. P. Singh, and H. Ulbricht, Models of wave-function collapse, underlying theories, and experimental tests, *Rev. Mod. Phys.* **85**, 471 (2013).
- [16] C. M. DeWitt and D. Rickles, *The role of gravitation in physics: report from the 1957 Chapel Hill Conference* (Edition Open Access, 2011).
- [17] L. Lami, J. S. Pedernales, and M. B. Plenio, Testing the quantumness of gravity without entanglement, *Phys. Rev. X* **14**, 021022 (2024).
- [18] H. Rudolph *et al.*, Force-gradient sensing and entanglement via feedback cooling of interacting nanoparticles, *Phys. Rev. Lett.* **129**, 193602 (2022).
- [19] T. Weiss, M. Roda-Llordes, E. Torrontegui, M. Aspelmeyer, and O. Romero-Isart, Large quantum delocalization of a levitated nanoparticle using optimal control: Applications for force sensing and entangling via weak forces, *Phys. Rev. Lett.* **127**, 023601 (2021).
- [20] M. Ludwig, K. Hammerer, and F. Marquardt, Entanglement of mechanical oscillators coupled to a nonequilibrium environment, *Phys. Rev. A* **82**, 012333 (2010).
- [21] A. F. Estrada and L. A. Pachón, Quantum limit for driven linear non-markovian open-quantum-systems, *New Journal of Physics* **17**, 033038 (2015).
- [22] F. Galve, L. A. Pachón, and D. Zueco, Bringing entanglement to the high temperature limit, *Phys. Rev. Lett.* **105**, 180501 (2010).
- [23] A. Szorkovszky, A. A. Clerk, A. C. Doherty, and W. P. Bowen, Mechanical entanglement via detuned parametric amplification, *New Journal of Physics* **16**, 063043 (2014).
- [24] Q. Lin, B. He, and M. Xiao, Entangling two macroscopic mechanical resonators at high temperature, *Phys. Rev. Applied* **13**, 034030 (2020).
- [25] A. Mari and J. Eisert, Gently modulating optomechanical systems, *Phys. Rev. Lett.* **103**, 213603 (2009).
- [26] F. Cosco, J. S. Pedernales, and M. B. Plenio, Enhanced force sensitivity and entanglement in periodically driven optomechanics, *Phys. Rev. A* **103**, L061501 (2021).
- [27] S. G. Hofer and K. Hammerer, Entanglement-enhanced time-continuous quantum control in optomechanics, *Phys. Rev. A* **91**, 033822 (2015).
- [28] K. Winkler, A. V. Zasedatelev, B. A. Stickler, U. Delić, A. Deutschmann-Olek, and M. Aspelmeyer, Steady-state entanglement of interacting masses in free space through optimal feedback control, arXiv (2024).
- [29] D. J. Heinzen and D. J. Wineland, Quantum-limited cooling and detection of radio-frequency oscillations by laser-cooled ions, *Phys. Rev. A* **42**, 2977 (1990).
- [30] L. Tian, M. S. Allman, and R. W. Simmonds, Parametric coupling between macroscopic quantum resonators, *New Journal of Physics* **10**, 115001 (2008).
- [31] R. F. Stengel, *Optimal control and estimation* (Courier Corporation, 1994).
- [32] J. Xiong, *An introduction to stochastic filtering theory*, Vol. 18 (OUP Oxford, 2008).
- [33] G. Adesso and F. Illuminati, Entanglement in continuous-variable systems: recent advances and current perspectives, *J. Phys. A* **40**, 7821 (2007).
- [34] G. Vidal and R. F. Werner, Computable measure of entanglement, *Phys. Rev. A* **65**, 032314 (2002).
- [35] J. Hench, C. Kenney, and A. Laub, Methods for the numerical integration of Hamiltonian systems, *Circuits Systems and Signal Process* **13**, 695–732 (1994).
- [36] M. Bukov, L. D'Alessio, and A. Polkovnikov, Universal high-frequency behavior of periodically driven systems: from dynamical stabilization to floquet engineering, *Adv. Phys.* **64**, 139 (2015).

- [37] A. Eckardt, Colloquium: Atomic quantum gases in periodically driven optical lattices, *Rev. Mod. Phys.* **89**, 011004 (2017).
- [38] M. S. Rudner and N. H. Lindner, Band structure engineering and non-equilibrium dynamics in Floquet topological insulators, *Nature Reviews Physics* **2**, 229–244 (2020).
- [39] M. S. Rudner and N. H. Lindner, The Floquet engineer’s handbook (2020), arXiv:2003.08252 [cond-mat.mes-hall].
- [40] A. W. Bojanczyk, G. H. Golub, and P. Van Dooren, Periodic Schur decomposition: algorithms and applications, in *Advanced Signal Processing Algorithms, Architectures, and Implementations III*, edited by F. T. Luk (SPIE, 1992).
- [41] D. Kressner, The periodic QR algorithm is a disguised QR algorithm, *Linear Algebra and its Applications* **417**, 423 (2006).
- [42] A. Varga, On solving periodic Riccati equations, *Numer. Linear Algebra Appl.* **15**, 809 (2008).
- [43] X. Ding and P. Cvitanović, Periodic eigendecomposition and its application to Kuramoto-Sivashinsky system (2015), arXiv:1406.4885 [nlin.CD].
- [44] J. Rieser *et al.*, Tunable light-induced dipole-dipole interaction between optically levitated nanoparticles, *Science* **377**, 987 (2022).
- [45] T. F. Roque and J. Roversi, Role of instabilities in the survival of quantum correlations, *Phys. Rev. A* **88**, 032114 (2013).